

# Interaction analysis of Continuous Slab Track (CST) on long-span continuous high-speed rail bridges

Gonglian Dai<sup>1a</sup>, Hao Ge<sup>\*1</sup>, Wenshuo Liu<sup>1b</sup> and Y. Frank Chen<sup>2,3a</sup>

<sup>1</sup>Department of Civil Engineering, Central South University, Changsha, China

<sup>2</sup>Department of Civil Engineering, Xijing University, Xian, China

<sup>3</sup>Department of Civil Engineering, Pennsylvania University, Middletown, USA

(Received January 3, 2017, Revised April 25, 2017, Accepted May 7, 2017)

**Abstract.** As a new type of ballastless track, longitudinal continuous slab track (CST) has been widely used in China. It can partly isolate the interaction between the ballastless track and the bridge and thus the rail expansion device would be unnecessary. Compared with the traditional track, CST is composed of multi layers of continuous structures and various connecting components. In order to investigate the performance of CST on a long-span bridge, the spatial finite element model considering each layer of the CST structure, connecting components, bridge, and subgrade is established and verified according to the theory of beam-rail interaction. The nonlinear resistance of materials between multilayer track structures is measured by experiments, while the temperature gradients of the bridge and CST are based on the long-term measured data. This study compares the force distribution rules of ballasted track and CST as respectively applied to a long span bridge. The effects of different damage conditions on CST structures are also discussed. The results show that the additional rail stress is small and the CST structure has a high safety factor under the measured temperature load. The rail expansion device can be cancelled when CST is adopted on the long span bridge. Beam end rotation caused by temperature gradient and vertical load will have a significant effect on the rail stress of CST. The additional flexure stress should be considered with the additional expansion stress simultaneously when the rail stress of CST requires to be checked. Both the maximum sliding friction coefficient of sliding layer and cracking condition of concrete plate should be considered to decide the arrangement of connecting components and the ultimate expansion span of the bridge when adopting CST.

**Keywords:** continuous slab track; continuous welded rail; long-span bridge; temperature gradient; damage conditions; additional rail stress

## 1. Introduction

High speed railway (HSR) has provided a great convenience for people to travel. It has the advantages of fast speed, large transport capacity, and environmental protection. Different countries have invented various types of HSR tracks. For example, France mainly applies ballasted tracks on HSR, Germany mainly adopts double-block type ballastless tracks such as Rheda and Zublin, and unit-plate type ballastless track is widely used in Japan (Liu *et al.* 2010).

China has adopted several types of ballastless tracks due to complex geographical condition and long HSR mileage. At the same time, in order to reduce the use of land and deformation of foundation and ensure the smoothness of railway line, bridges account for a large proportion of the HSR lines in China. For example, Shanghai-Kunming and Beijing-Shanghai HSR lines, both adopting the CST, have the bridge proportion of 88% and 80% respectively. As the

HSR lines extend, more and more long-span concrete bridges have been constructed to cross the rivers and valleys (Hu *et al.* 2014).

The increase in bridge span has a negative effect on the rail due to its expansion effect. According to the UIC code (International Union of Railways 2001), when the CWR on the bridge was not equipped with rail expansion device (RED), the maximum expansion span was restricted to 60m for steel bridges and 90m for concrete bridges. In 2003, The Ministry of Railways of China (2003) issued the interim code for design of CWR on newly built railway bridges, which suggested that the maximum expansion spans of 100 m and 120 m for steel bridges and concrete bridges, respectively, or the RED should be set on the CWR.

The long span bridges are widely built with the increase of HSR mileage. In addition, the requirements for rail smoothness increase as the train speeds goes up. TB 10015-2012 (2012) of China suggested that the rail expansion device should be less used on the CWR. As a new type of ballastless track applied only in China, CST aims to reduce the interaction between the bridge and the upper rail by setting up the sliding layer between them. As a result, it can achieve the situation that a RED is not necessarily needed on a long-span bridge. However, the CST is more complex and the track system on the bridge is composed of rail, track plate, and base plate.

\*Corresponding author, Ph.D. Student  
E-mail: [csubridgehao@163.com](mailto:csubridgehao@163.com)

<sup>a</sup>Professor

<sup>b</sup>Lecturer

E-mail: [liuwenshuo@scu.edu.cn](mailto:liuwenshuo@scu.edu.cn)

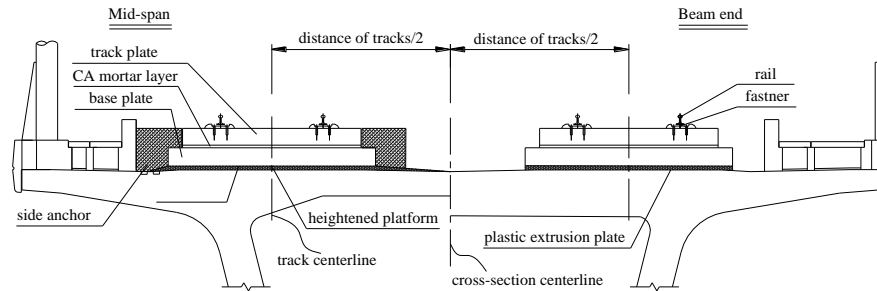


Fig. 1 Structural system of CST on bridge

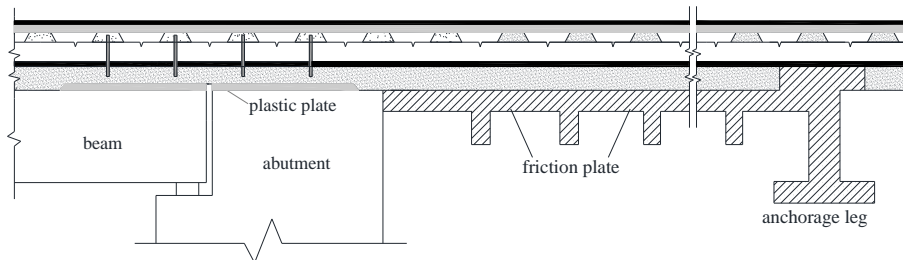


Fig. 2 The friction plate and anchorage leg

The majority of researches have been done on the interaction between bridge and rail. Ruge *et al.* (2007 and 2009) analyzed the nonlinear resistance characteristics of ballasted railway and their influences on the CWR longitudinal force. However, his models did not consider the influence of multi span bridges and there was only one layer of constraint condition between bridge and rail. While the CST structure has multi-layer structure and different constraint conditions. In addition, there are connecting components between concrete plate and bridge in the beam gap. Jia (2010) established the FE model for the CST on a multi span simply supported beam bridge and analyzed the influence of different parameters on the mechanical performance of the track system. Zeng (2015) investigated the random vibration characteristic of interaction system of train-slab track-simply supported girder bridge with fifteen spans by using the pseudo-excitation method. But the research on the force distribution of CST on a long-span bridge is relatively less.

Long-span bridges have a large expansion length. Although the sliding layer is set to reduce the expansion effect of the bridge, it cannot completely eliminate the influence of bridge expansion on the upper track structure. The constraint resistances between structural layers are different. And the connecting components at the beam gap will have concentrated effect on track structure. That all would add the complexity of the interaction between bridge and CST.

Li *et al.* (2015) has established three dimensional model of CST ballastless track on a long span concrete bridge and the mechanical properties of the track system on bridges with different spans were compared. The effects of various structural parameters on the stress and deformation of CST on long span bridges were studied by Cai *et al.* (2011). In their study, they selected the uniform temperature variation as the temperature load, based on experience, but did not consider the temperature gradient of bridge and concrete

plate (Aleksandrova 2016).

Based on the interaction theory of beam and rail, this study establishes the FE model to calculate the longitudinal additional force of the CST on the long-span bridge, and the temperature load and key parameters are valued respectively according to the experiments. The influences of sliding layer service performance and the concrete plate cracking are also discussed.

## 2. Interaction model for CST and long-span bridge

### 2.1 Structural system and mechanical principle of CST

In order to avoid the use of compensating plate on the bridge and accelerate the construction progress, a new ballastless track scheme on the long bridge was put forward. Different from the traditional ballastless track, the track plate and base plate of CST are continuous structure along the whole line including the bridge. It abandons the design principle that the CWR on the long bridge must be equipped with RED and breaks at the bridge gap.

The CST on the bridge is composed of multilayer structures including rail, elastic fastener, prefabricated track plate, cement asphalt mortar (CA mortar), base plate, and sliding layers (see Fig. 1).

Friction plate and anchorage leg are set on the subgrade to eliminate the additional longitudinal force of the track structure that is caused by the bridge expansion. They can prevent the additional force from affecting the rail on the subgrade (see Fig. 2).

To reduce the influence of bridge expansion on the track structure, the sliding layer composed of two pieces of geotechnical cloth and a piece of membrane are arranged between bridge and base plate. It can release the

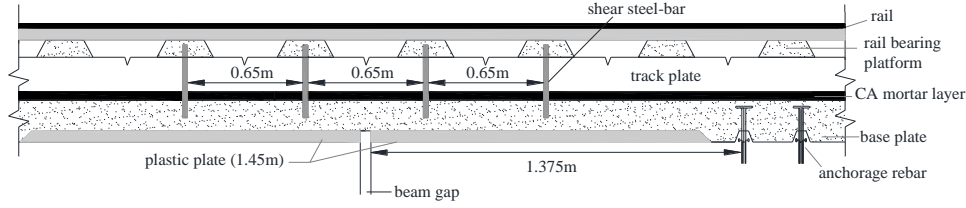


Fig. 3 Track structures and connecting components

longitudinal force transferred from the bridge to the upper track structure, so that the RED may be eliminated even for a long span bridge (see Fig. 3).

As the sliding layer cannot transfer the longitudinal force totally, the anchorage rebars are preset at the beam end above the fixed support. They are used to consolidate the base plate with the bridge and thus can transfer the braking force of upper track structures to the fixed support directly (Fig. 3). Anchorage reinforcement consists of two rows of fourteen HRB335 steel bars with the diameter of 28 mm.

In addition, shear steel-bars are set at the beam gaps and anchorage legs to make the track plate and base plate act together ensuring their adaptation to the deformation there (Fig. 3).

Plastic plate with high strength is set above the beam end (Fig. 3). Under the effect of vehicular load and temperature gradient, the bridge will warp at both ends. In order to weaken the influence of rotation of beam ends, the plastic plate is set within 1.45 m away from beam end, it can achieve the situation of deformation buffer.

## 2.2 Finite element (FE) model

According to the structural characteristics of the CST on a bridge, this study establishes the integrated model of rail-track plate-base plate-beam-pier to calculate the forces of CST. As the track plate and base plate are longitudinal continuous along the whole line, this model adopts the beam element with the section information to simulate rail, track structure, bridge, and subgrade support layer. The section parameters and material properties of each component are determined according to the actual situation.

According to International Union of Railways (2001) and TB 10015-2012 (2012), the resistance of rail fastener should adopt a nonlinear resistance model. The resistance of WJ-8 type fasteners adopted in CST is determined by Eq. (1) according to the Chinese code (TB 10015-2012 2012).

$$r_{fastener}(kN) = \begin{cases} 7.5u & u \leq u_0 = 2mm \\ 15 & u > u_0 = 2mm \end{cases} \quad (1)$$

The resistance of sliding friction layer is simulated using nonlinear springs. Hu *et al.* (2008) conducted experiments on sliding friction coefficient and concluded that the friction coefficient of regular sliding layer varied from 0.2 to 0.3 and 0.3 is used in the model. Two layers of geotechnical cloth without membrane are paved between friction plate and upper base plate to absorb the additional longitudinal force of the track structure on the bridge. In this situation,

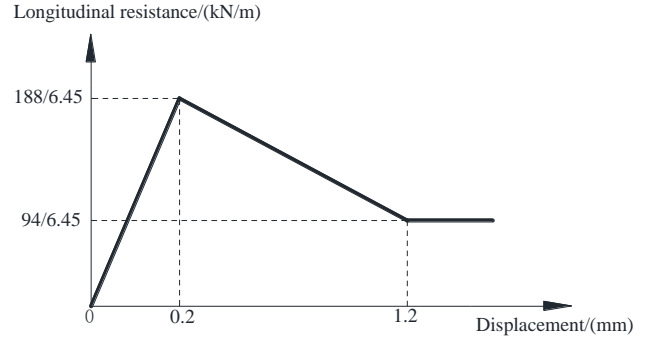


Fig. 4 Resistance of CA mortar layer

the frictional coefficient is found to be between 0.5 and 0.8 and 0.7 is valued in the model. The corresponding critical slip displacement is 0.5 mm.

The prefabricated plate has a length of 6.45 m. Based on the repeated push plate experiments by Dai *et al.* (2016), the limiting resistance of CA mortar under each track plate was about 188 kN corresponding to the deformation displacement of 0.2 mm. The resistance of CA mortar layer then decreased until the deformation displacement reached 1.2 mm when a shear failure occurred in the CA mortar layer, the base plate and track plate were in the state of sliding friction. The sliding frictional resistance was about 94 kN. Therefore, the CA mortar resistance model could be simplified as shown in Fig. 4.

$$r_{ca\ mortar\ layer}(kN/m) = \begin{cases} 29.1u/0.2 & u \leq u_0 = 0.2mm \\ 29.1(1.2-u) & u_0 < u < u_1 = 1.2mm \\ 14.6 & u > u_1 = 1.2mm \end{cases} \quad (2)$$

According to The Third Railway Survey and Design Institute Group Corporation (2009), the minimum compressive stiffness per meter of the plastic plate shall not be less than 413 kN/mm. We selected the spring with compressive stiffness of 500 kN/mm to simulate the plastic plate.

Linear springs with equivalent stiffness are used to simulate the anchorage rebars, shear steel-bars, and

Table 1 Comparison of calculation results

Contents	Chen (2012)	This model	Error rate
Maximum additional force of rail (kN)	343.37	361.98	5.4%
Maximum additional force of plate (kN)	579.81	592.5	2.2%
Maximum additional force of pier (kN)	862.28	807.2	6.4%
Maximum displacement of continuous beam (mm)	29.79	30.74	3.2%

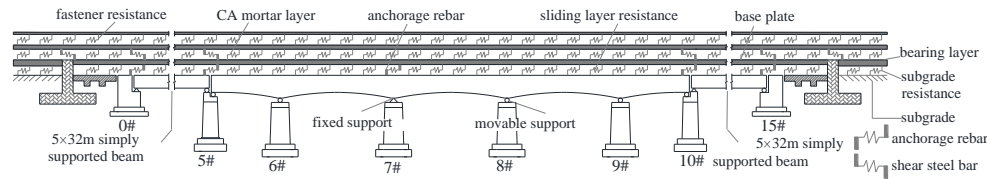


Fig. 5 Schematic diagram of bridge-CST interaction model

Table 2 Long span bridges adopting CST

Bridge	Span (m)	HSR line	Expansion span (m)
Lian shui Bridge	60+3×100+60	Hangzhou-Changsha	260
Huai he Bridge	48+5×80+48	Beijing-Shanghai	320
Cao e jiang Bridge	76+3×120+76	Hangzhou-Ningbo	316
Jing hua jiang Bridge	75+4×135+75	Hangzhou-Changsha	378
Xin jiang Bridge	72+3×116+72	Hangzhou-Changsha	304

anchorage legs. The model is adopted to calculate the the example presented in Chen (2012) using the same parameters. The error is found to be less than 6.4% and the model is thus considered capable of simulating the interaction between bridge and CST (Table 1).

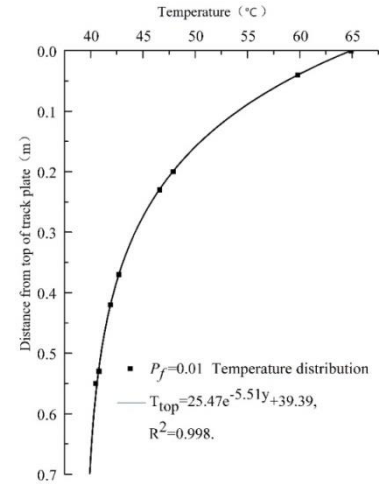
### 2.3 CST on long-bridge

With the extension of HSR lines in China, both the number and span of long-span bridges are increasing significantly. Current long span continuous bridges adopting CST and without RED are summarized in Table 2.

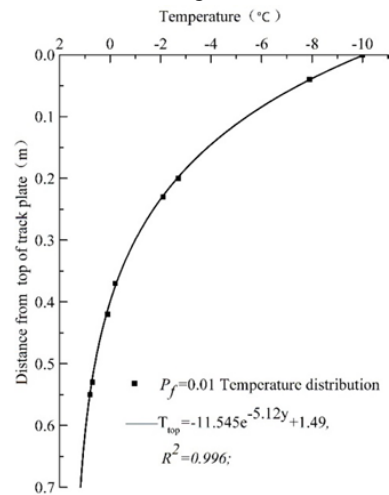
Taking the Lianshui long-span bridge of Shanghai-Kunming HSR line as an example. The long-span continuous beam of 60 m+3×100 m+60 m is located in the middle and the 5×32 m simply supported beams were respectively set on both sides. The bridge has a total length of 740 m and its maximum expansion span reaches 260 m. The fixed beam support is arranged on the left side for the simply supported beam and at 7# pier for the continuous beam (Fig. 5). The 50 m long friction plate and 100 m long subgrade section are both established behind the bridge abutment in the FE model to reduce the influence of boundary conditions.

### 2.4 Temperature gradient mode

It is critical to select a reliable load model to calculate the force of the track structure. TB 10015-2012 (2012) stipulated that the annual temperature change of concrete bridges adopting ballastless track was  $\pm 30^\circ\text{C}/\text{m}$ . International Union of Railways (2001) suggested the uniform temperature change of a bridge was  $\pm 35^\circ\text{C}/\text{m}$ . Both the specifications did not consider the temperature gradient of bridge. According to the TB 10621-2009 (2009), the annual temperature change of the ballastless concrete plate was determined based on the local meteorological conditions, the positive temperature gradient valued at  $90^\circ\text{C}/\text{m}$  and the negative temperature gradient at  $45^\circ\text{C}/\text{m}$ . In



(a) Heating condition



(b) Cooling condition

Fig. 6 Temperature gradient of track plate and base plate

selected the site near the studied example and embedded the temperature sensors into the corresponding section positions to make a long-term temperature test on the box beam and ballastless concrete plate (Dai *et al.* 2015, Ye *et al.* 2013, 2016). According to the statistical analysis from the two-year temperature field data collected, a nonlinear temperature gradient model is developed for the box girder, track plate, and base plate with the exceedance probability of 0.01 (Figs. 6-7).  $20^\circ\text{C}$  is selected as the closure temperature according to TB 10621-2009 (2009).

### 3. Interaction analysis of CST

The CWR stresses of ballasted track and CST are

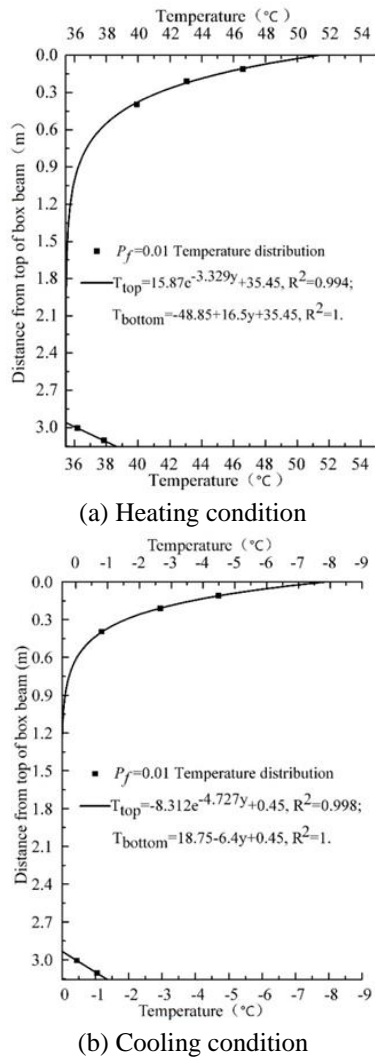


Fig. 7 Temperature gradient of box beam

Table 3 Maximum rail additional stress and specification limits

Results		Maximum additional compressive stress (MPa)	Maximum additional tensile stress (MPa)
Heating condition	Ballasted track	122	37.7
	CST	9.89	7.03
Cooling condition	Ballasted track	42.5	126
	CST	6.98	6.91
Limiting value of UIC		72	92
Limiting value of China specification		61	81

compared when they are respectively laid on the long span bridge without the RED. The longitudinal resistance of ballasted track is available in TB 10015-2012 (2012).

In the charts showing the results, the location of fixed support of continuous girder bridge is selected as the origin of horizontal coordinate. Displacement to the right is positive, tension is positive, and pressure is negative.

### 3.1 Rail stress distribution of ballasted track and CST

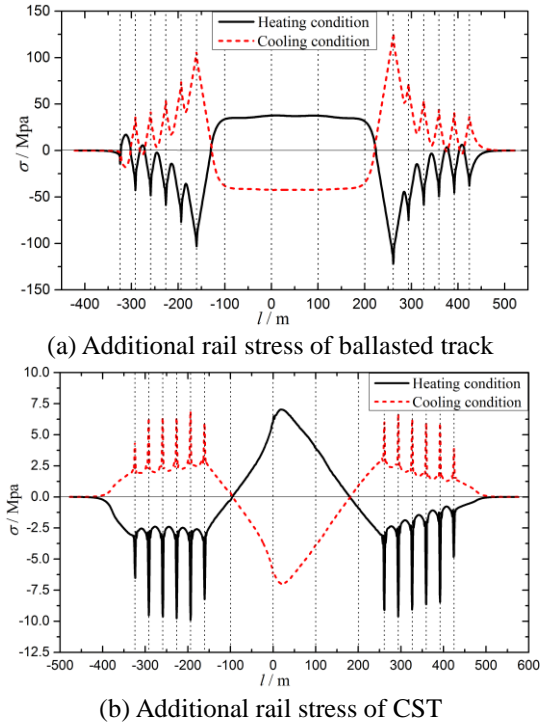


Fig. 8 Additional rail stresses of ballasted track and CST

The rail additional stresses of ballasted and CST under the measured temperature loads are shown in Fig. 8.

According to the calculated results, the rail longitudinal stress of ballasted track is obviously greater than that of CST. International Union of Railways (2001) stipulated that the maximum value of additional rail compressive stress should be less than 72 MPa and that of the additional tensile stress should be less than 92 MPa. The limiting compressive stress and tensile stress stated in the Ministry of Railways of China (2004) were respectively 61 MPa and 81 MPa. The maximum additional rail stress and the specification limits are shown in Table 3. It can be known that the RED is necessary when adopting ballasted track on a long bridge and it is possible to set CST on long span bridges without using a RED.

At the beam gaps, there have significant changes in the longitudinal rail stress of CST and the maximum change value can be as high as 6.2 MPa (see Fig. 8). The reason for this phenomenon is that the connecting components such as shear steel-bars and anchorage rebars existing at the beam gaps can increase the effect of bridge deflection on the upper rail. According to TB 10015-2012 (2012) for CWR, there is no need to consider both the expansion stress and the flexure stress. However, this suggestion does not apply to the CWR of CST. When the additional rail stress of CST is checked, the additional flexure stress caused by both temperature gradient and vertical load should be considered.

When ballasted track is laid, the maximum additional stress occurs at the free end of the continuous beam. The maximum stress depends on the factors such as expansion span, bridge temperature variation, and the resistance of fastener. There is additional stress platform occurring in the intermediate range of the continuous beam (Fig. 8(a)). The longitudinal rail displacement is consistent with that of the

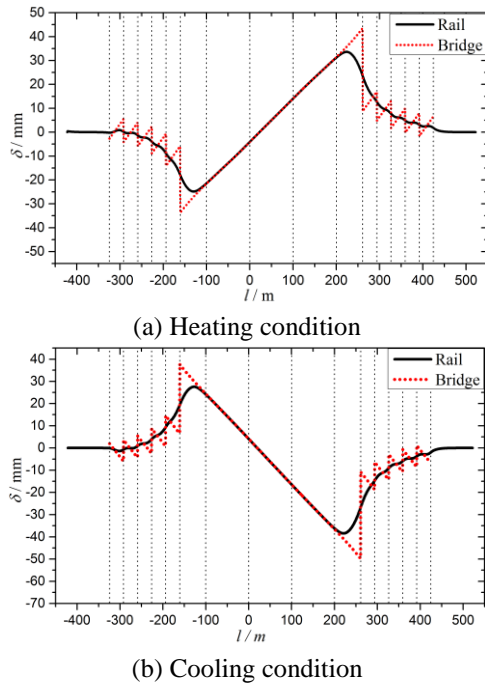


Fig. 9 Longitudinal displacements of rail and bridge (ballasted track)

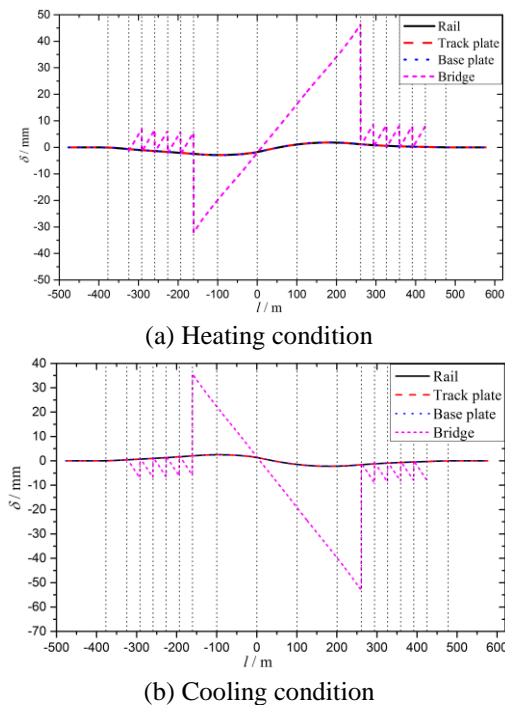
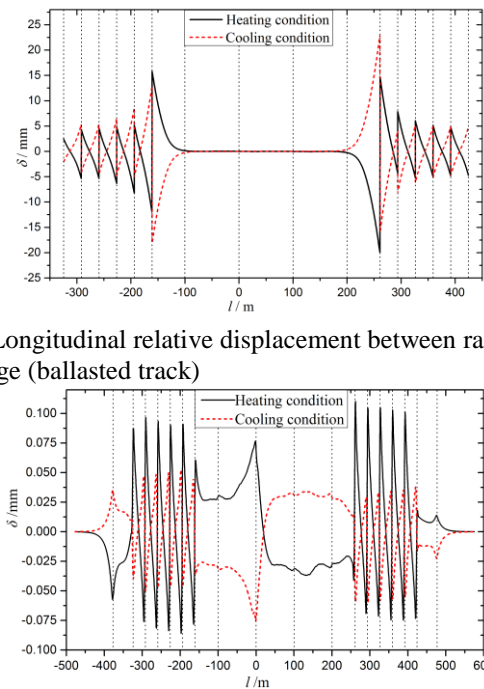


Fig. 10 Longitudinal displacements of rail and track plate of CST

bridge (Fig. 9). So, the fastener has no resistance and the rail additional stress is constant. It was also referred as “coordination zone” (Li Y 2012). Wei *et al.* (2015) had proved the stress platform by experiments.

When the bridge is separated from the CST by the sliding layer. As shown in Fig. 10, the longitudinal displacement of the bridge is large and the upper track structures suffer small longitudinal displacements.



(a) Longitudinal relative displacement between rail and bridge (ballasted track)

(b) Longitudinal relative displacement between rail and track plate (CST)

Fig. 11 Longitudinal relative displacements between rail and bridge/track plate

Meanwhile, the displacement of each layer is nearly the same (Fig. 10). Different from the ballasted track, the additional longitudinal stress of CST rail depends on the longitudinal relative displacement between rail and track plate, as shown in Fig. 11. Although the fastener resistance of CST is greater than that of ballasted track, the additional rail stress is much smaller due to the small relative displacement between its rail and track plate. The maximum relative displacement is only 0.12 mm which is far less than the fastener’s plastic critical displacement of 2 mm.

### 3.2 Force of connecting components

The anchorage rebars and shear steel-bars are set at the beam gaps to transfer the longitudinal force and adapt to the rotational deformation. The forces of these connecting components should also be considered to ensure the safety of the CST system.

Under the effect of measured temperature mode, anchorage rebars bear small vertical tension and big longitudinal force, the maximum longitudinal force is 749.6 kN appearing at the fixed support of the continuous bridge, Fu (2008) studied the anchorage rebars and found the ultimate capacity of 2800 kN that is far above 749.6 kN. The maximum vertical and longitudinal forces of one single shear rebar are 13.5 kN and 27 kN, respectively. It is noted that the beam-end rotation has a certain influence on the unity of track plate and base plate, but the maximum force of the single shear rebar is far less than its ultimate strength. The rail and connecting component of CST have a high safety factor under the effect of measured temperature mode.

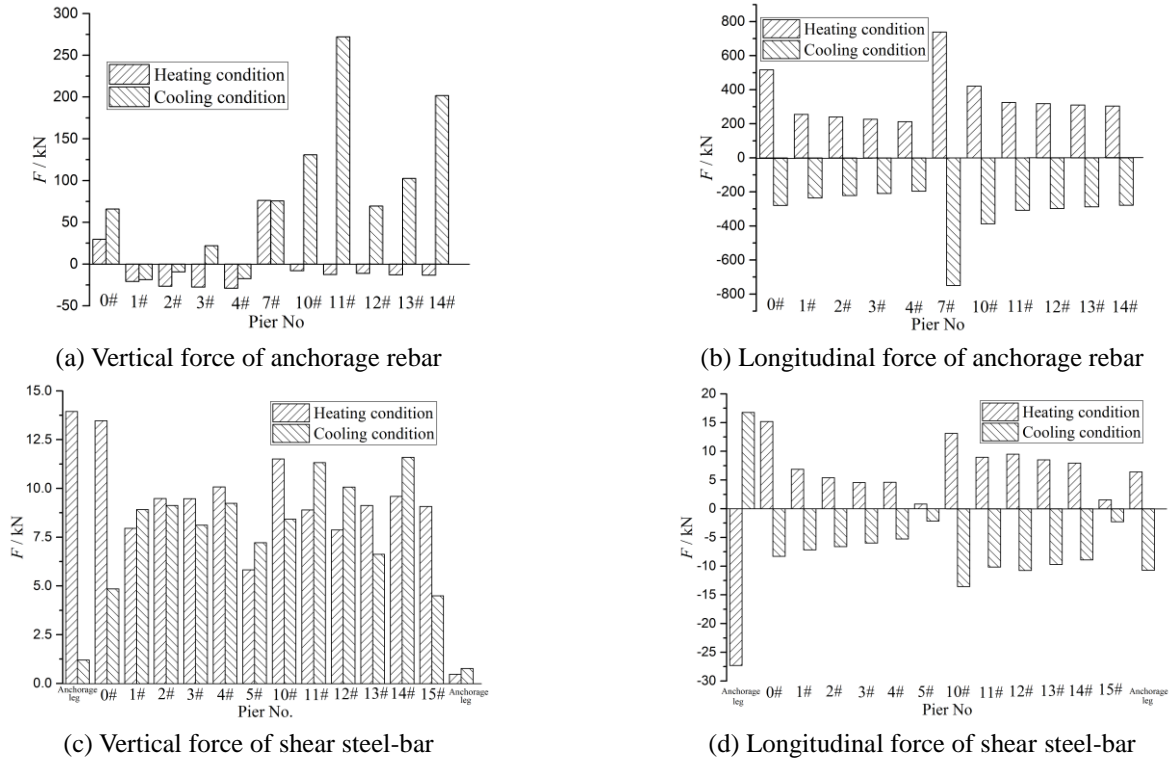


Fig. 12 Forces of CST connecting components

Table 4 Friction coefficients of sliding layer tested under different serving conditions

No.	Concrete surface of bridge	Materials	Average thrust	Friction coefficient
1	Scraped	Geotechnical cloth	7.5kN	0.82
2	Sand-blasted surface	Two layers of fiber cloth	6.8kN	0.74
3	Scraped	One layer of fiber cloth and one layer of membrane	3.2kN	0.35
4	Sand-blasted surface	One layer of fiber cloth and one layer of membrane	1.9kN	0.21
5	Surface brushed waterproof paint	-	3.8kN	0.41
6	Surface brushed waterproof paint	One layer of fiber	5.1kN	0.55

#### 4. Interaction analysis of CST under damage conditions

##### 4.1 Sliding friction layer

The friction coefficient of the sliding layer varies from 0.2 to 0.3 in the intact state. However, the two fabrics and one membrane will be gradually damaged with the increasing service time, and the increasing friction coefficient will leads to the increase in the longitudinal rail force.

As shown in Table 4, sliding layers were stimulated under different states in Landkreis Neumarkt, Germany in 2005 and the corresponding friction coefficients were obtained. According to the data, when only one layer of

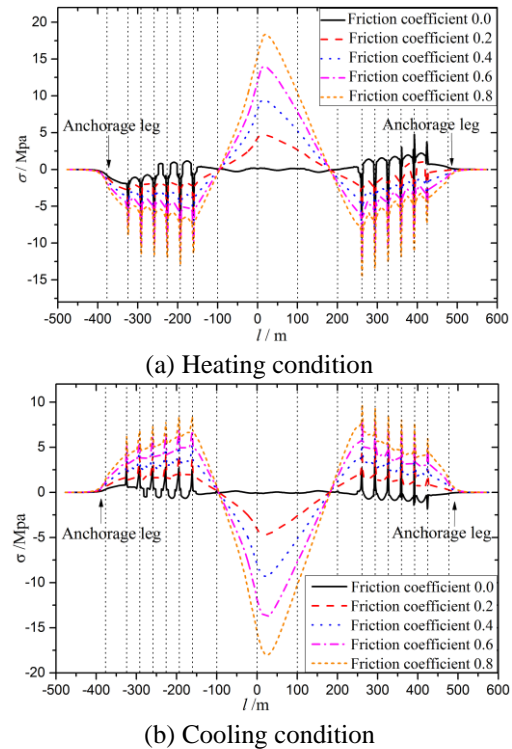
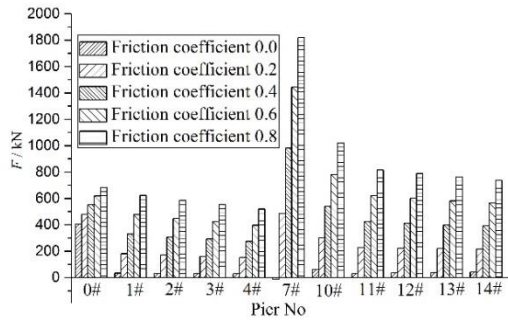


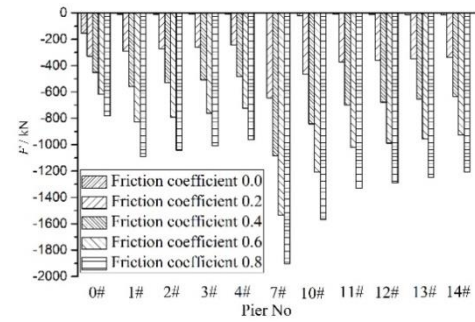
Fig. 13 Additional rail stress of CST with different sliding friction coefficients

cloth works, the sliding friction coefficient could reach 0.84 (Hu S.T *et al.* 2008). A series of friction coefficients including 0, 0.2, 0.4, 0.6, and 0.8 are taken to assess the influence on the force of CST.

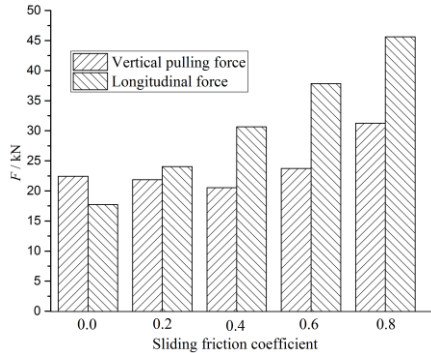
In Fig. 13, when the friction coefficient is 0, there is



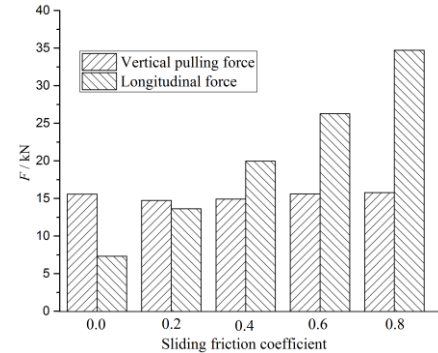
(a) Longitudinal force of anchorage rebar under heating condition



(b) Longitudinal force of anchorage rebar under cooling condition



(c) Force of shear steel-bar under heating condition



(d) Force of shear steel-bar under cooling condition

Fig. 14 Forces of connecting components with the friction coefficients varying from 0 to 0.8

virtually no additional rail stress apart from the rail at the beam gaps. The bridge would bend under the effect of temperature gradient and the additional rail stress of the beam gaps is caused by the beam end rotation.

Additional rail stress exists along the whole lines when the sliding friction is considered. With the sliding friction coefficient increases from 0 to 0.8, the maximum additional compressive stress increases significantly from 7.2 MPa to 14.7 MPa, while the maximum additional tensile stress increases from 4.8 MPa to 18.4 MPa under the heating condition. Under the cooling condition, the maximum additional compressive stress increases from 1.85 MPa to 18 MPa and the maximum additional tensile stress increases from 3.8 MPa to 9.8 MPa.

The forces of connecting components are shown in Fig. 14. As the sliding friction coefficient increases, the longitudinal forces of anchorage rebar and shear steel-bars increase significantly and the vertical forces remain approximately the same. When the sliding friction coefficient increases from 0.0 to 0.8, the maximum longitudinal force of anchorage rebar increases from 406.4 kN to 1818.9 kN under heating condition and increases more than 10 times to 1897.2 kN under cooling condition. The maximum longitudinal force of the shear steel-bars increases quite significantly also. The most undesirable sliding friction coefficient should be considered when designing the expansion span of a long-span bridge and the connecting components of CST.

#### 4.2 Cracking of concrete plate

The CST ballastless concrete plate would crack under

the effect of cooling temperature. For example, the concrete elastic modulus of the base plate is  $3.0 \times 10^4$  MPa and the coefficient of expansion is  $1.0 \times 10^{-5}/^\circ\text{C}$ . When the cooling temperature exceeds  $4.8^\circ\text{C}$ , the concrete tensile stress is larger than its tensile strength of 1.43 MPa and it will crack. The cracked concrete plate reduces the expansion stiffness and ability to transfer the longitudinal forces, thus affecting the distribution of longitudinal forces in a track structure.

The relationship between axial force and temperature variation is described by Eq. (2) and the effective expansion stiffness of the concrete is defined in Eq. (3). So, the relationship between the effective elastic modulus and cooling temperature variation can be expressed by Eq. (4)

$$N = EA\alpha\Delta T \quad (2)$$

$$E_{eff}A_c = E_cA_c + E_sA_s \quad (3)$$

$$E_{eff} = \begin{cases} E_c \left( 1 + \frac{E_s}{E_c} \rho \right) & (\Delta T < \frac{f_t}{\alpha\Delta T}) \\ \frac{f_t}{\alpha\Delta T} + E_s \rho & (\Delta T > \frac{f_t}{\alpha\Delta T}) \end{cases} \quad (4)$$

In the above,  $\rho$  is the reinforcement ratio,  $E_{eff}$  is concrete effective elastic modulus,  $\alpha$  is the concrete expansion coefficient,  $\Delta T$  is the cooling temperature variation, and  $f_t$  is the concrete tensile strength.

It can be noted that before the concrete cracking, the effective elastic modulus is irrelevant to the cooling temperature variation. After cracking appears, the effective elastic modulus is inversely proportional to the temperature drop range.

Substituting the material parameters of track plate and

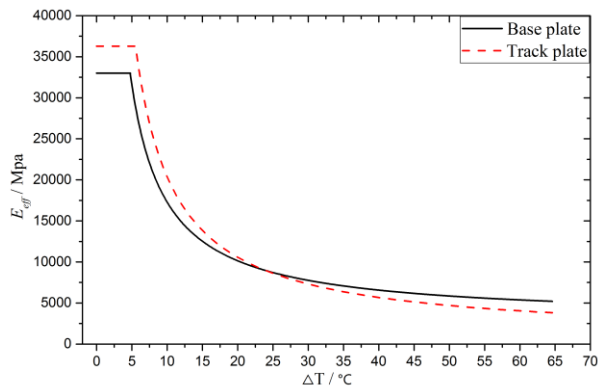
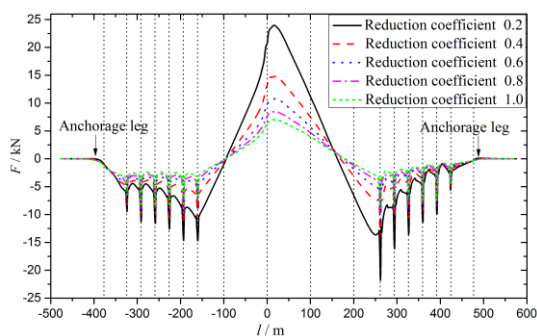
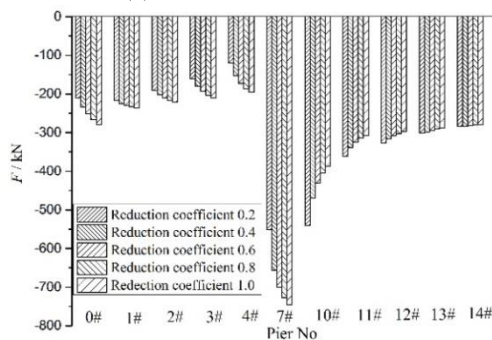


Fig. 15 Curves of concrete plate effective elastic modulus versus cooling temperature



(a) Additional rail stress

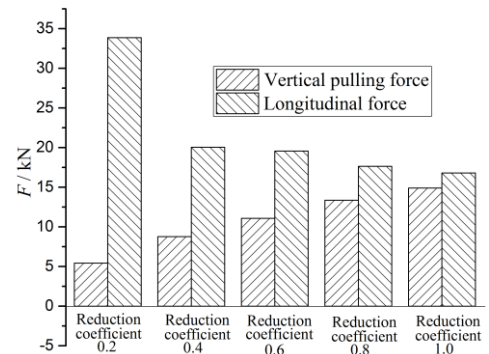


(b) Longitudinal force of anchorage rebar

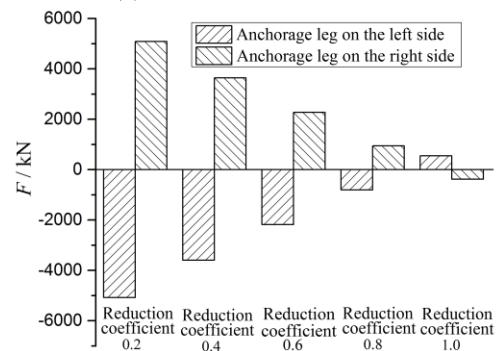
Fig. 16 Forces of CST with different reduced stiffness coefficients

base plate into Eq. (4), and the curves of effective elastic modulus versus temperature are obtained (Fig. 15). When the temperature of track plate drops  $39.7^{\circ}\text{C}$  and that of base plate drops  $30.1^{\circ}\text{C}$ , their effective elastic moduli reduce to about 20% of the initial elastic moduli. Therefore, the reduced expansion stiffness coefficients of the concrete plate vary from 0.2 to 1.0. As the cracks will close when the temperature rises, this study selects the measured cooling temperature model to calculate the forces of the track structure (Ren *et al.* 2011).

According to the calculated results (Fig. 16), the additional rail stress increases with decreasing concrete plate expansion stiffness. The bridge expansion effect is transferred from the bottom structures to the top structures. When the concrete plate cracks and reduces in stiffness, the additional force it withstand will decrease, resulting in



(c) Force of shear steel-bar



(d) Longitudinal force of anchorage leg

Fig. 16 Continued

increasing additional rail stress. Under the measured cooling temperature condition, when the stiffness reduction coefficient of the concrete plate drops to 0.2 from 1, the maximum additional rail stress increases to 24 MPa from 6.9 MPa and the maximum additional tensile stress increases to 15.9 MPa from 5.9 MPa.

As the concrete plate reduces in expansion stiffness, the longitudinal force of the anchorage rebars decreases, while that of the shear steel-bars increases. The anchorage rebars connects the base plate with the bridge at the beam end. When the base plate reduces its stiffness, the anchorage rebars reduce their longitudinal forces correspondingly under the effect of the same beam-end rotation. The shear steel-bars are set to connect the track plate with the base plate at the beam end. They are similar to CWR and do not displace under the effect of self temperature. Only when affected by the bridge expansion, they will experience longitudinal displacements. When they reduce in stiffness, the longitudinal relative displacement between them will increase under the same bridge expansion which will consequently result in increasing shear rebar forces. It is thus noted that the arrangement of the anchorage rebars should be based on the situation that there is no crack and the setting of shear steel-bars should be calculated based on the ultimate cracking state.

Anchorage leg is set to anchor the extra additional force of the rail on the bridge and eliminate the influence of the bridge expansion on the subgrade rail. When concrete plate reduces in stiffness, the additional force it transferred will decrease and correspondingly the additional force that anchorage leg needs to anchor increases. When the reduction coefficient reduces to 0.2 from 1.0, the

longitudinal force carried by the left anchorage leg increases to 5078 kN from 552 kN and the right anchorage leg's bearing capacity increases to 5092 kN from 380.9 kN. The additional rail stress at the rear of the anchorage rebar is 0.0 for different reduction coefficients. Thus it is known that the anchorage leg can effectively anchor the additional longitudinal stress of the track structure on the bridge regardless of the concrete state.

## 5. Conclusions

The force distribution rules of CST on long span bridges and the influences of different damage conditions are analyzed based on the measured temperature model and structural parameters. Based on this study, the following conclusions may be drawn:

- Compared with ballasted track, when CST is adopted on a long span bridge, the additional rail stress is small and the use of RED on the CWR is unnecessary.
- Under the measured temperature loads, track structures and connecting components of CST on a long-span bridge will have a high safety factor.
- Different from the ballasted track, when the beam end deflects, the additional rail stress of CST increases significantly at the beam ends because of the effect caused by the rigid connecting components there. TB 10015-2012 (2012) holds that the additional expansion stress and flexure stress needn't to be considered simultaneously when checking the rail stress of CWR. However, the additional rail flexure stress caused by bridge temperature gradient and vertical load should be considered with the expansion stress when checking the CST rail stress.
- With the increase of the sliding friction coefficient, the additional rail stress and longitudinal forces of anchorage rebars and shear steel-bars increase significantly. It is suggested that the damage of the sliding layer and the most undesirable friction coefficient be considered to decide the maximum expansion span of the bridge and the arrangement of connecting components.
- The cracking of CST concrete plate will lead to obvious increase in the additional stress of the rail on a long-span bridge. The anchorage rebar force decreases, while the shear rebar force increases as the concrete plate reduces its expansion stiffness. It is suggested that the maximum bridge expansion span and the shear steel-bar be designed based on the ultimate cracking condition of the concrete plate.

## Acknowledgments

The research described in this paper was financially supported by the Natural Science Foundation of China (Project 51378503), the Fundamental Research Funds for the Central Universities of Central South University (2016zzts076) and the Project (2015M570687) supported by China Postdoctoral Science Foundation

## References

- Aleksandrova, N.N. (2016), "Effect of thermal gradients on stress/strain distributions in a thin circular symmetric plate", *Struct. Eng. Mech.*, **58**(4), 627-639.
- Cai, X.P., Gao, L., Sun, H.W. and Qu, C. (2011) "Analysis on the mechanical properties of longitudinally connected ballastless track continuously welded rail on bridge", *China Railw. Sci.*, **32**(6), 28-33.
- Chen, X.P. (2012), "Analysis on influencing factors of additional expansion and contraction forces between CRTSII slab ballastless track and long-span continuous beam bridge", *J. Fuzhou Univ.*, **40**(3), 383-387.
- Dai, G.L. and Su, M. (2016), "Full-scale field experimental investigation on the interfacial shear capacity of continuous slab track structure", *Arch. Civ. Mech. Eng.*, **16**(3), 485-493.
- Dai, G.L., Su, H.T. and Yan, b. (2015), "Experimental study on the vertical temperature gradient of longitudinally connected slab ballastless track on bridge in autumn", *J. Hunan Univ.*, **42**(3), 94-99.
- Fu, X.J. (2008), "Reasonable pier stiffness of CRTS II Ballastless track on bridge", Master Dissertation, Southwest Jiaotong University, Chengdu.
- Hu, S.T., Liu, W.B. and Jiang, Z.Q. (2008), *Summary of Design Principle and Method of CRTS II Slab Ballastless Track in Beijing-Tianjin City Railway*, China Academy of Railway Sciences, Beijing, China.
- International Union of Railways (UIC) (2001), *Track/Bridge Interaction Recommendations for Calculations*, Paris, France.
- Jia, M.X. (2010), "Influential factors analysis of longitudinal force in bridges with CRTSII-type slab ballastless track", Master. Dissertation, Southwest Jiaotong University, Chengdu.
- Li, D.S., Niu, B. and Hu, S.T. (2016), "Mechanical properties of CRTS II slab ballastless track on long temperature span concrete bridge", *China Railw. Sci.*, **37**(3), 22-28.
- Li, Y. (2012), "Study on variation rules of longitudinal force of continuous welded rails on long-span cable-stayed bridge", *J. Railw. Eng. Soc.*, **10**(10), 42-46.
- Liu, X.Y., Zhao, P.C., Yang, R.S. and Wang, P. (2010), *Theory and Method of Unballasted Track of Passenger Dedicated Line*, Southwest Jiao Tong University Press, Chengdu, Sichuan, China.
- Ministry of Railways of China (2003), *Interim Code for Design of Railway Continuously Welded Rail on The Newly Built Railway Bridge*, China Railway Publishing House, Beijing, China.
- Ministry of Railways of China (2004), *Interim Code for Design of Beijing-Shanghai High Speed Railway*, China Railway Publishing House, Beijing, China.
- Nan, H., Dai, G.L., Bin, Y. and Ke, L. (2014), "Recent development of design and construction of medium and long span high-speed railway bridges in China", *Eng. Struct.*, **74**, 233-241.
- Ren, J.J., Wang, P. and Liu, X.Y. (2011), "Influencing factors of temperature force and displacement of longitudinally coupled ballastless welded turnout on bridges of dedicated passenger lines", *J. China Railw. Soc.*, **2**(33), 79-85.
- Ruge, P. and Birk, C. (2007), "Longitudinal forces in continuously welded rails on bridge decks due to nonlinear track-bridge interaction", *Comput. Struct.*, **85**(7/8), 458-475.
- Ruge, P., Widarda, D.R., Schmalzlin, G. and Bagayoko, L. (2009), "Longitudinal track-bridge interaction due to sudden change of coupling interface", *Comput. Struct.*, **87**, 47-58.
- TB 10015-2012 (2012), *Code for Design of Railway Continuously Welded Rail*, China Railway Publishing House, Beijing, China.
- TB 10621-2009 (2009), *Code for Design of High-speed Railway*, China Railway Publishing House, Beijing, China.
- The Third Railway Survey and Design Institute Group

- Corporation (2009), *Technical Specification for High Strength Plastic Plate of CRTS II Slab Ballastless Track of Passenger Dedicated Railway*, China Academy of Railway Sciences, Beijing, China.
- Wei, X.K., Zhou, Y., Liu, H. and Wang, P. (2015), "Theoretical and experimental study on longitudinal interaction of CWR on railway cable-stayed bridge", *Railw. Stand. Des.*, **59**(8), 62-67.
- Ye, X.W., Ni, Y.Q. and Yin, J.H. (2013), "Safety monitoring of railway tunnel construction using FBG sensing technology", *Adv. Struct. Eng.*, **16**(8), 1401-1409.
- Ye, X.W., Su, Y.H., Xi, P.S., Chen, B. and Han, J.P. (2016), "Statistical analysis and probabilistic modeling of WIM monitoring data of an instrumented arch bridge", *Smart Struct. Syst.*, **17**(6), 1087-1105.
- Zeng, Z.P., He, X.F., Zhao, Y.G., Yu, Z.W., Chen, L.K., Xu, W.T. and Lou, P. (2015), "Random vibration analysis of train-slab track-bridge coupling system under earthquakes", *Struct. Eng. Mech.*, **54**(5), 1017-1044.